OPEN ACCESS

GAVIN PUBLISHERS

Nanomedicine and Nanoscience Research

Research Article

Fujiwara T, et al. J Nanomed Nanosci: JNAN-146.

DOI: 10.29011/2577-1477.100046

Nanorobotic Manipulation of Thin-film Graphite Sheet for 3D Cubic Structures

Takafumi Fujiwara[1*], Masahiro Nakajima[2], Yasuhisa Hasegawa[2], Toshio Fukuda[1,3], Huang Qiang,[3]

[1]Faculty of Science and Engineering, Meijo University, Japan

[2]Department of Micro-Nano Mechanical Science and Engineering, Nagoya University, Nagoya, Aichi, Japan

[3]Intelligent Robotics Institute, School of Mechatronic Engineering, Beijing Institute of Technology, China

[*]**Corresponding author:** Takafumi Fujiwara, Faculty of Science and Engineering, Meijo University, Nagoya, Aichi, Japan. Tel: +81528382603; Email: 153435035@ccalumni.meijo-u.ac.jp

Citation: Fujiwara T, Nakajima M, Hasegawa Y, Fukuda T, Huang Q (2018) Nanorobotic Manipulation of Thin-film Graphite Sheet for 3D Cubic Structures. J Nanomed Nanosci: JNAN-146. DOI: 10.29011/2577-1477.100046

Received Date: 05 June, 2018; **Accepted Date:** 28 June, 2018; **Published Date:** 04 July, 2018

Abstract

A thin-film graphite sheet was manipulated for 3D cubic structures by nanorobotic manipulation inside an electron microscope. A cubic net of thin-film graphite sheet was designed and fabricated by Focused Ion Beam (FIB) etching for bending manipulation. Groove lines were designed and etched by FIB to bend at a desired position. Then, each surface of cubic net was bent to form a cubic 3D structure. In this paper, the bending stress was measured using a silicon cantilever to determine the elastic and plastic deformation regions for the bending manipulation. From the experimental results, the yield points are changed depending on the thickness of the groove lines for the thin-film graphite sheet.

Keywords: 3D Cubic Structures; Bending Stress Measurement; Groove Lines; Nanorobotic Manipulation; Thin-Film Graphite

Introduction

Graphene comprises carbon atoms with a sheet-like nanostructure. It has received a great deal of attention after being separated from graphite by a simple scotch tape method in 2004 [1]. Researches on graphene-based catalysts [2,3] and electric devices [4,5], were conducted for applications recently. It has various excellent physical properties such as mechanical strength [6], mechanical conductivity [7], and thermal conductivity [8]. Until now, various applications in Nanoelectromechanical System (NEMS) using graphene have been proposed such as optical interferometers [9], photovoltaic devices [10], and LC circuits [11]. Some sensors and actuator require Three-Dimensional (3D) structure. Fabricating to 3D structure, such as Origami-inspired construction of 3D microstructures [12] and fabrication of 3D structure using FIB stress introduced deformation [13] etc. Extending the Two-Dimensional (2D) structure of graphene into a 3D structure would make it useful for integration into a 3D NEMS.

To achieve a 3D thin-film graphite structure from 2D thin-film graphite, we propose to use a Nanomanipulation technique. We have previously worked on 3D Nanomanipulation of carbon nanotubes inside a Scanning Electron Microscope (SEM) [14] and a Transmission Electron Microscope (TEM) [15]; the SEM enables us to obtain an almost real-time observation in 3D space. A nanorobotics approach was recently developed to handle 2D thin-film graphite structures using SEM Nanomanipulation [16]. However, it is challenging to achieve a 3D graphene structure by integrating 1) lifting, 2) bending, 3) cutting, and 4) Nanomanipulation-based bonding techniques.

To obtain a 2D patterned thin-film graphite structure, some etching techniques are required to fabricate a designed shape. For example, direct mechanical force [17] and electrochemical etching techniques [18] were demonstrated to selectively etch thin-film graphite. In these techniques, a probe is needed, and it is not easy to fabricate relatively complicated 2D patterned thin- film graphite structures. On the other hand, an ion beam was used to obtain 2D patterning effectively [19]. This technique is widely used for micro/nanofabrication and is useful for fabricating 2D patterns thin-film graphite structures with arbitrary shapes. Additionally, it is easy to change the etching depth depending on the dose rate of the ion beam on the sample.

On the other hand, the mechanical evaluation of thin-film graphite was performed using Atomic Force Microscope (AFM) manipulation. The Young's modulus of monolayer graphene was determined as 1 TPa and the breaking strength is 42 N/m [20]. For polycrystalline graphene, the membrane has a 53 GPa maximum failure stress [21], and the shear stress is revealed by a similar technique [22]. Evaluation of the mechanical stress of graphene was performed using elastic silicone substrates [23]. However, the bending stress of thin-film graphite was not investigated in previous work. Since the bending stress is important for 3D manipulation, effective bending was especially considered in our design by adding groove lines on the thin-film graphite to determine the bending lines by concentration of the bending stress.

In this paper, we propose a fabrication strategy to turn 2D thin-film graphite into a 3D cubic structure using Nanomanipulation. Figure 1 shows the bending process of a thin-film graphite sheet. Figure 1a shows a thin-film graphite sheet.

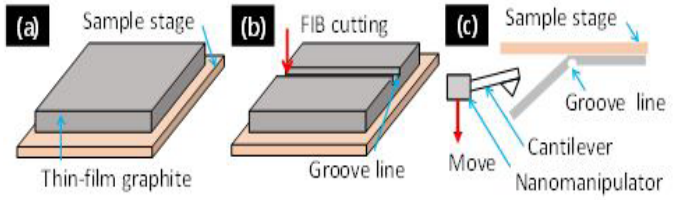

Figures 1(a-c): Bending process of thin-film graphite sheet. **(a)** Thin-film graphite sheet. **(b)** Fabrication of the groove line by FIB. **(c)** Measurement of thin-film graphite bending force by a silicone cantilever based on nanorobotics manipulation.

A thin-film graphite specimen was fixed on the sample stage. Figure 1b shows that the thin-film graphite was cut into arbitrary shapes and grooved to facilitate bending by FIB. Figure 1c shows that the bending force of the thin-film graphite was measured using a cantilever. A Nanomanipulator with three degrees of freedom was used to handle the end effectors in a coordinated manner. The Nanomanipulator was installed inside a Field-Emission Scanning Electron Microscope (FE-SEM) for high resolution observation in a 3D space. A 2D cubic net of thin-film graphite was designed and fabricated using FIB etching. Each surface of the cubic net was bent to form a 3D cubic structure. The bending stress was also measured by bending manipulation of the surface of the cubic net using a silicon cantilever.

The advantage of our approach is that the 3D thin-film graphite structure is obtained by simple bending process like an Origami using a manipulator. The Origami processing method is considered to be an effective method for fabrication of 3D various micro-nano structures [12]. In addition, basically, the thin-film graphite sheet has a structure formed by multilayered graphene, which has advantageous such as simple fabrication process as same as graphene, easy to handle for Nanomanipulation and easily obtainable.

Experimental Equipment and Procedures for Bending Thin-film Graphite Using a Nanomanipulation System

NanoManipulation System Inside FESEM

We used a nanorobotic manipulation system inside a FESEM for lifting and bending thin-film graphite. Figure 2a shows a schematic diagram of the nanomanipulation system inside a FESEM chamber. It comprises a sample stage for placing a thin-film graphite sample and a nanomanipulator with 3 translational degrees of freedom. A tungsten probe for bending the thin-film graphite is attached to the nanomanipulator. Figure 2b shows a photo of the nanomanipulation system in the FESEM. The thin-film graphite was prepared using the scotch tape method from highly oriented pyrolytic graphite [1]. To facilitate nanomanipulation, the thin-film graphite was fixed on the sample stage inclined at 60°.

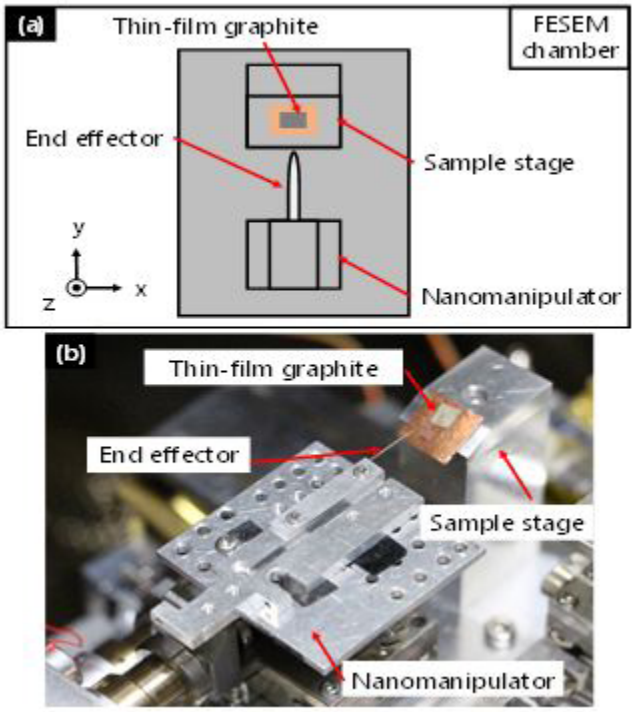

Figures 2(a,b): Experimental set-up of Nanomanipulation system inside FESEM. **(a)** Schematic diagram of Nanomanipulation system in FESEM (top view). **(b)** Overview photo of Nanomanipulation system in FESEM.

Preparation of End Effector by Tungsten Probe

To lift up the thin-film graphite sheet, an end effector was prepared using FIB. A tungsten probe 1 μm in tip diameter was

attached to the nanomanipulator as an end effector. If the cubic surface was lifted with the tungsten probe directly, the thin-film graphite would be damaged because the tip of the tungsten probe is too sharp. In this study, the size of the tungsten probe was adjusted for the cubic net design to maintain the contact area. The width of the tungsten probe was determined by the FIB etching process to be 10 μm; this size is same as the width of one cubic surface). The thickness of the tungsten probe was thinned to about 5 μm to avoid contact with the sample substrate.

SEM images of the fabricated tungsten probe are shown in Figure 3. Figure 3a shows the tungsten probe before fabrication, and top and side views of the fabricated tungsten probe are shown in Figure 3b and Figure 3c, respectively.

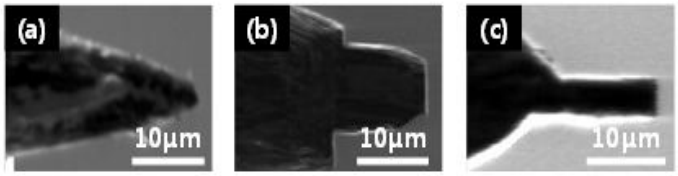

Figures 3(a-c): SEM images of fabricated tungsten probe. **(a)** Before fabrication of tungsten probe. **(b)** Top view of the fabricated tungsten probe. **(c)** Side view of the fabricated tungsten probe.

Preparation of 2D Thin-film Graphite Structure

At first, a thin-film graphite cubic net was prepared using FIB etching. The design is shown in Figure 4a; the width and length of one cubic surface were designed to be 10 μm. For bending the thin-film graphite net in the perpendicular direction, it is important to decide on a groove line. Hence, FIB etching was operated under two conditions; the outer lines were etched at a dose amount of 5900 × 10^{15} ion/cm^2 to cut the thin-film graphite fully, and the boundary of each surface was etched at a dose amount of 590 × 10^{15} ion/cm^2 to form the groove line. The fabricated thin-film graphite cubic net is shown in Figure 4b. The net was cut to form a surface of box structure with a groove line.

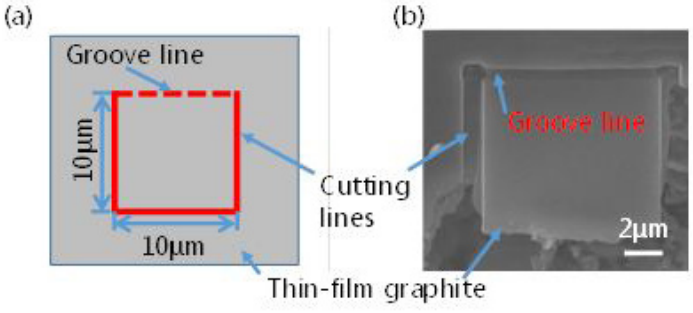

Figure 4(a, b): Fabrication of patterned thin-film graphite. **(a)** Schematic of patterning of thin-film graphite. **(b)** SEM images of fabricated patterned thin-film graphite.

Bending Procedure of Thin-film Graphite

In order to change the thickness of the groove lines, the fabrication amount of thin-film graphite was measured for different dose amounts of the FIB. Figure 5 shows the SEM images of the fabricated thin-film graphite trench. The cross section area of thin-film graphite trench was measured for different dose amount of FIB. Each fabricated amount was 0.07 μm^2 (Figure 5 a), 0.05 μm^2 (Figure 5 b), 0.04 μm^2 (Figure 5c), 0.03 μm^2 (Figure 5d), 0.02 μm^2 (Figure 5e), and 0.01 μm^2 (Figure 5f). Figure 6 shows the cross section area of fabricated thin-film graphite trench by different doze amount. This result indicates that a linear relationship between the fabricated amount and the dose amount (1.0 × 10^{-4}μm^2 /(10^{15}ion/cm^2)).

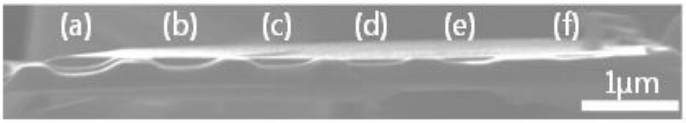

Figures 5(a-f): Fabrication results of thin-film graphite by different dose amounts of FIB. **(a)** Dose amount: 590 × 10^{15} ion/cm^2. **(b)** Dose amount: 492 × 10^{15} ion/cm^2. **(c)** Dose amount: 393 × 10^{15} ion/cm^2. **(d)** Dose amount: 295 × 10^{15} ion/cm^2. **(e)** Dose amount: 197 × 10^{15} ion/cm^2. **(f)** Dose amount: 98 × 10^{15} ion/cm^2.

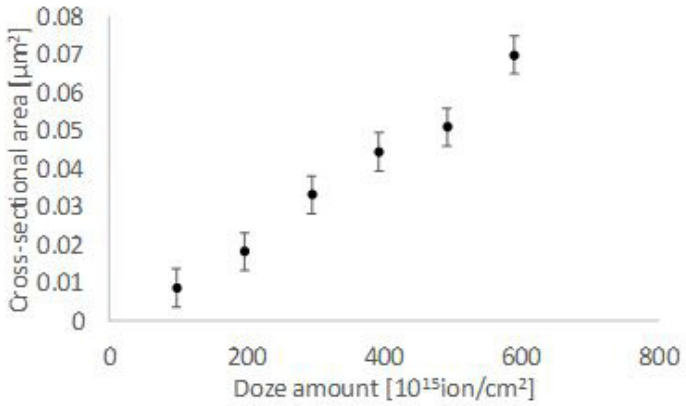

Figure 6: Cross section area of the fabricated trench of thin-film graphite by different doze amount.

For bending stress analysis, the thin-film graphite is required to be lifted up. The lifting-up and measurement processes are shown in Figure 7. At first, a single surface of the cubic net design was prepared by FIB etching (Figure 7a). When lifting the single surface of thin-film graphite, a groove line was formed (Figure 7b). Figure 7c shows the release of the probe. Thin-film graphite is lifted by plastic deformation, making the measurement with a cantilever easier.

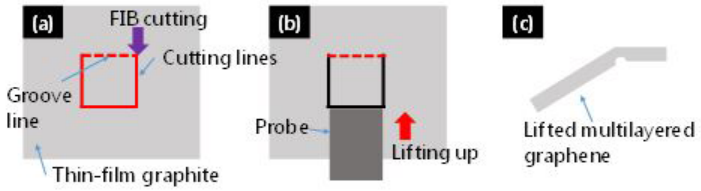

Figures 7(a-c): Schematic diagrams of lifting up process. **(a)** Cutting thin-film graphite by FIB. **(b)** During lifting up. **(c)** After lifting up (side view).

Bending Stress Measurement of Thin-film Graphite by Cantilever

Calculation of Bending Stress at the Groove Line of Thin-film Graphite

The bending stress of one cubic surface was measured using a silicon cantilever, and the bending force was calculated according to Hooke's law. The applied force of the cantilever tip, F, to the thin-film graphite is given by Hooke's law as

$$F = k\varphi \cdot \frac{2}{3} \cdot L_c \qquad (1)$$

Where k is the spring constant of the cantilever, φ is the angle of the cantilever, and L_c is the length of the cantilever. The applied stress to the thin-film graphite surface, σ, is written as

$$\sigma = \frac{M}{Z} = \frac{F \cdot L_G}{b \cdot h^2/6} \qquad (2)$$

Where M is the applied bending moment to the thin-film graphite, Z is the section modulus of the thin-film graphite, F is the applied force on the thin-film graphite, and L_G, b, and h are the length, thickness, and width of the thin-film graphite, respectively. When the bending moment is applied to the thin-film graphite with a groove line, the applied stress is concentrated on the thinnest part of the groove line. The bending stress of thin-film graphite with a groove line is written as

$$\sigma_g = \frac{F \cdot L_G}{b_g \cdot h_g^2/6} \qquad (3)$$

Where b_g and h_g are the thickness and width of thin-film graphite at the groove line, respectively. From this equation, the concentration of bending stress is estimated.

Experimental Procedure of Bending Stress Measurement of Thin-Film Graphite

In this experiment, three types of silicon cantilever were used depending on the amount of bending stress applied. The spring constant was 0.61 N/m with a length of 100 μm, 0.16 N/m with a length of 200 μm, and 0.02 N/m with a length of 200 μm. Calibration experiment was conducted with the resonant oscillation by applying electrostatic forces for the AFM cantilevers. The relative errors of the resonant oscillations of the cantilever were 7%, 10% and 6%. It can be said that the value is correct because the relative error is as low as 10% or less. The single surface of the cubic net design was fabricated by FIB etching, as shown in Figure 7. The dimensions are 10 μm cube edge length, 0.6 μm thick, thin-film graphite, and 0.5 μm thick groove lines. Figure 8 shows a typical example of the lifting process of a single cubic surface. The thin-film graphite before and after lifting up is shown in Figure 8a and Figure 8b, respectively. Figure 8c shows a side view of the lifted-up thin-film graphite by rotating it 90° in the SEM chamber.

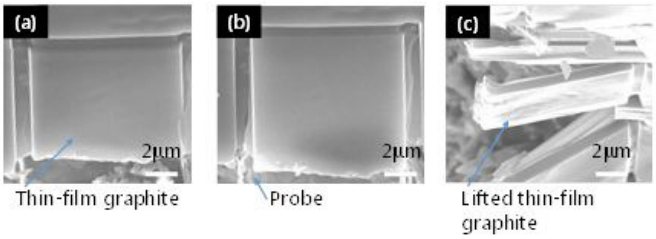

Figures 8(a-c): Experimental results of lifting up process of thin-film graphite. **(a)** Before lifting up. **(b)** During lifting up. **(c)** After lifting up (side view).

To evaluate the amount of plastic deformation for different thicknesses of groove lines, the bending stress is measured for a single cubic surface of the thin-film graphite. A schematic diagram of the bending stress measurement is shown in Figure 9. At first, the single cubic surface is lifted up at an initial angle as shown in Figure 9a. The lifted thin-film graphite is bent step-by-step using a Nanomanipulator, and the applied bending force is measured by a silicon cantilever (Figure 9b). The bending angles of the thin-film graphite and the cantilever are measured from the SEM images. After releasing the silicon cantilever from the thin-film graphite, the thin-film graphite is bent by plastic deformation (Figure 9c). In this experiment, bending stress of thicknesses of three groove lines was measured. Each measurement was repeated three times to obtain the amount of deformation after bending.

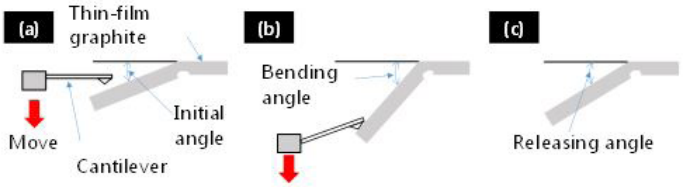

Figures 9(a-c): Schematic diagrams of bending stress measurement. **(a)** Before measurement. **(b)** Bending force measurement from cantilever deflection. **(c)** After measurement.

Experimental Results of Bending Stress Measurement of Thin-film Graphite

Figure 10 shows the experimental results of the bending stress analysis for the single cubic surface (h_g: 0.2 μm first time). Figure 10a shows thin-film graphite before applying the bending force. Initial angle was 32.8˚. The thin-film graphite was bent using the silicon cantilever (spring constant: 0.02 N/m) by moving it in the horizontal direction Figure 10b. The released thin-film graphite is shown in Figure 10c. The angle of the thin-film graphite was 35.2˚ after releasing from the maximum angle of 51.4˚. Figure 11 shows the experimental results of a bending stress diagram for a groove line thickness of 0.2 μm. The bending process was repeated three times to the same thin-film graphite sheet. As shown in Figure 11, the thin-film graphite sheet was bent elastically. Under this experimental condition, the plastic deformation was 1.8 ± 0.5˚ on an average in the three times bending processes. The increase in the first and second bending stress was linear. The angle of bending after release returned to the starting angle. Hence, the bending is considered to be in the elastic region for a groove line thickness of 0.2 μm.

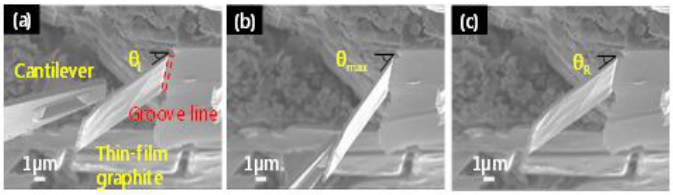

Figures 10(a-c): SEM images of bending stress measurement using a silicon cantilever (Thickness of groove line: 0.2 μm). (a) Before measurement bending force (Initial angle: 32.8˚). **(b)** During bending force measurement (Bending angle: 51.4˚). **(c)** After measurement (Bending angle: 35.2˚).

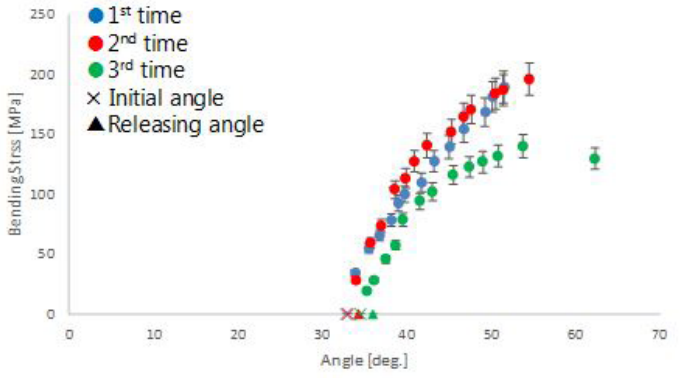

Figure 11: Bending stress diagram depending on bending angle of thin-film graphite (Thickness of groove line: 0.2 μm).

Figure 12 shows the experimental results of the bending stress analysis for the single cubic surface (h_g: 0.4 μm first time). Figure 12 a shows thin-film graphite before applying the bending force. The initial angle was 17.5˚. The thin-film graphite was bent using the silicone cantilever (spring constant: 0.16 N/m) by moving in the horizontal direction (Figure 12b). The angle was bent up to 54.1˚. The released thin-film graphite is shown in Figure 12c. Releasing angle is 21.4˚. Figure 13 shows the experimental results of bending stress diagram for a groove line thickness of 0.4 μm. The bending process was repeated three times to the same thin-film graphite sheet. As shown in Figure 13, the thin-film graphite sheet was bent elastically. Under this experimental condition, the plastic deformation was 2.2 ± 1.7˚ on an average in the three times bending processes. Although the plastic deformation amount is larger than 0.2 μm, it has returned to almost the original angle. Hence, the bending is considered to be in the elastic region for a groove line thickness of 0.4 μm.

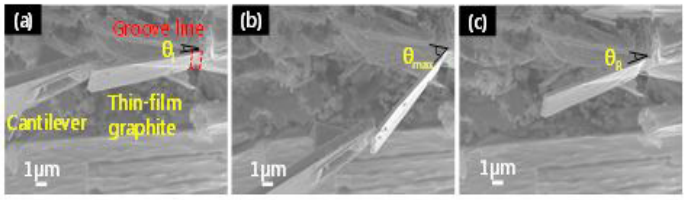

Figures 12(a-c): SEM images of bending stress measurement using a silicon cantilever (Thickness of groove line: 0.4 μm). **(a)** Before measurement bending force (Initial angle: 17.5˚). **(b)** During bending force measurement (Bending angle: 54.1˚). **(c)** After measurement (Bending angle: 21.4˚).

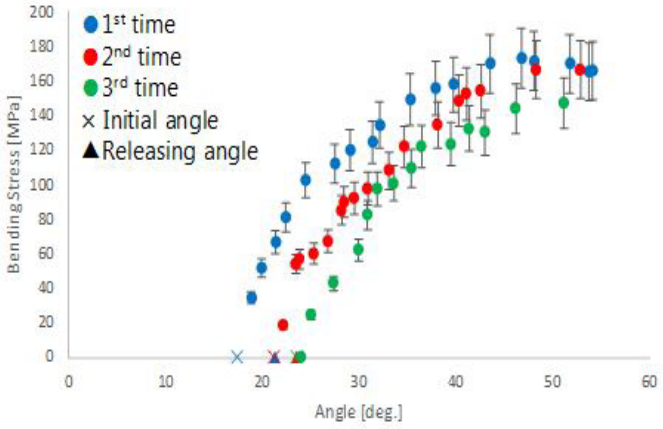

Figure 13: Bending stress diagram depending on bending angle of thin-film graphite (Thickness of groove line: 0.4 μm).

Figure 14 shows the experimental results of the bending stress analysis for the single cubic surface (h_g: 0.5 μm first time). Figure 14a shows thin-film graphite before applying the bending force. Initial angle was 3.6˚. The thin-film graphite was bent using the silicone cantilever (spring constant: 0.61 N/m) by moving in the horizontal direction (Figure 14b). The released thin-film graphite is shown in Figure 14c, was bent up to 50.8˚, and became

22.5° after release. Figure 15 shows the experimental results of bending stress diagram for a groove line thickness of 0.5 μm. The bending process was repeated three times to the same thin-film graphite sheet. As shown in Figure 15, the thin-film graphite sheet was bent elastically. Under this experimental condition, the plastic deformation was 13.1 ± 5.9° on average in the three times bending processes. It was greatly plastic deformed than before. The bending stress gradually changed after a linear increase. Hence, plastic deformation occurred under this experimental condition for a groove line thickness of 0.5 μm.

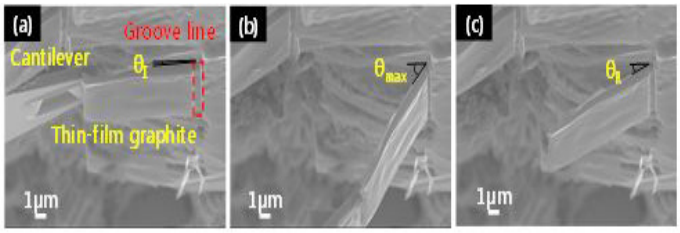

Figures 14(a-c): SEM images of bending stress measurement using a silicon cantilever (Thickness of groove line: 0.5 μm). **(a)** Before measurement bending force (Initial angle: 3.6°). **(b)** During bending force measurement (Bending angle: 50.8°). **(c)** After measurement (Bending angle: 22.5°).

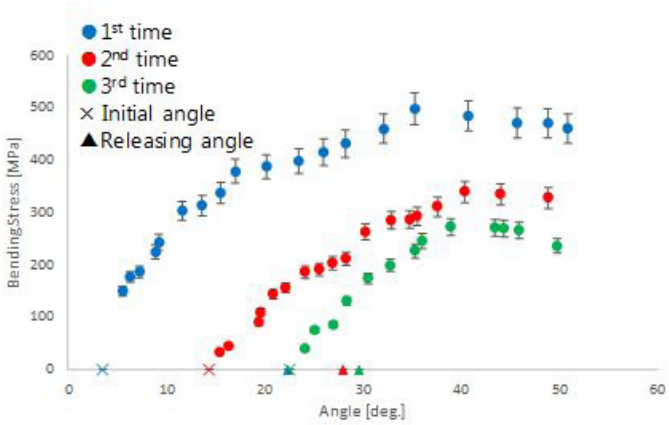

Figure 15: Bending stress diagram depending on bending angle of thin-film graphite (Thickness of groove line: 0.5 μm).

Table 1 shows a summary of experimental data obtained by the bending stress measurement for each thickness of a groove line with an initial angle, a maximum angle, an angle after releasing, an angle difference by plastic deformation, an applied force at maximum angle, and a bending stress at maximum angle. When the thickness of the groove line was increased, the amount of plastic deformation was also increased. As shown in Figure 11 and 13, the bending stress diagram shows an almost linear relationship for a groove line thicknesses at 0.2 μm and 0.4 μm. On the other hand, as shown in Figure 15, the bending stress diagram shows a non-linear relationship for the groove line thickness at 0.5 μm. As summarized in this table, these results show that the bending was in the elastic deformation region for the thicknesses at 0.2 μm and 0.4 μm, whereas the bending was in the plastic deformation region for the thickness at 0.5 μm. From these results, to perform a bending process using plastic deformation, it is necessary to conduct the bending with the thickness of the groove line of 0.5 μm or more.

Groove line thickness [μm]	Bending time	Initial angle (θ_I) [deg.]	Maximum angle (θ_{max}) [deg.]	Releasing angle (θ_R) [deg.]	Angle difference by plastic deformation [deg.]	Applied force at maximum angle [μN]	Bending stress at maximum angle [MPa]
0.2	1	32.8	51.4	35.2	2.4	1.5	189.3
	2	32.7	54.5	34.4	1.6	1.5	206.9
	3	34.5	62.3	36.1	1.5	1.0	129.6
0.4	1	17.5	54.1	21.4	3.9	5.0	165.5
	2	21.3	52.9	23.6	2.3	4.8	166.0
	3	23.6	51.1	24.1	0.5	4.4	146.8
0.5	1	3.6	50.8	22.5	18.8	21.2	459.5
	2	14.4	48.8	28.0	13.6	13.8	326.9
	3	22.6	49.7	29.6	7.0	10.2	235.9

Table 1: Angle differences by plastic deformation for each groove line thickness.

Table 2 shows the bending stress at the same bending angle for each thickness of groove line. This value is calculated from the approximated curves for each bending process obtained by the least squares method. From this result, the bending stress was higher when the thickness increased as the applied force was increased. The plastic deformation occurred due to the high bending stress by bending of the thick groove line that is higher than 0.5 μm under approximately 60° bending angles.

Groove line thickness [μm]	Bending time	Bending angle 35 deg. [MPa]	Bending angle 40 deg. [MPa]	Bending angle 45 deg. [MPa]	Bending angle 50 deg. [MPa]
0.2	1	42.1	98.8	144.0	177.6
	2	43.6	112.1	159.0	184.4
	3	15.4	71.8	111.9	135.8
0.4	1	149.0	165.1	172.4	170.7
	2	124.9	147.3	160.8	165.5
	3	106.5	130.9	143.0	143.0
0.5	1	489.0	492.1	479.0	449.7
	2	294.6	322.5	334.0	329.0
	3	230.5	265.8	267.8	236.3

Table 2: Bending stress for each groove line thickness of groove lines at different bending angles.

Fabrication of Three-Dimensional Structures of Thin-film Graphite

Based on the above technique, thin-film graphite was selectively bent into a 3D cubic structure from a 2D cubic net design as shown schematically in Figure 16. Four groove lines were fabricated to determine the bending position of the cubic net for a 3D cubic structure. Each surface was bent individually using nanomanipulation.

Experimental Procedure of Fabrication of 3D Structure of Thin-film Graphite

A cubic net design of thin-film graphite was fabricated by FIB etching experimentally as same as previous sections (Figure 16a). Grooves were fabricated on the multilayered graphene surface by FIB etching to act as groove lines (Figure 16a). One of the surfaces of the cubic net was bent by the end effector of a nanomanipulator (Figure 16c). The second, third and fourth surfaces of the cubic net were bent in the same way (Figure 16d and 16e). A cubic 3D structure of thin-film graphite was fabricated by bending process at the groove lines (Figure 16f).

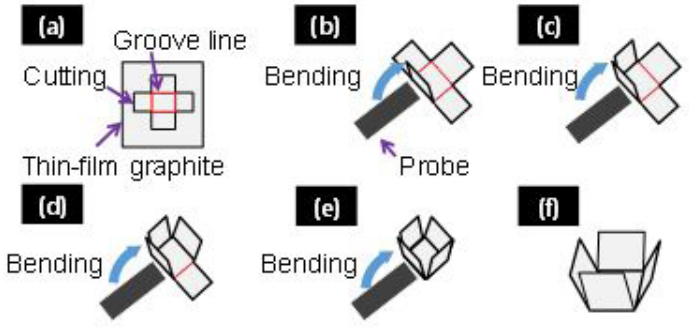

Figures 16(a-f): Schematic of fabrication process 3D cubic structure of thin-film graphite. **(a)** Cutting as a cubic net design by FIB. **(b)** Bending of the one surface of the cubic net. **(c)** Bending of the second surface of the cubic net. **(d)** Bending of the third surface of the cubic net. **(e)** Bending of the fourth surface of the cubic net. **(f)** Fabricated 3D cubic structure by plastic deformation based on nanorobotic manipulation.

Experimental Result of Fabrication of 3D Structure of Thin-film Graphite

Figure 17 shows the fabrication result of the thin-film graphite cubic structure. A net of thin-film graphite that becomes a box with a square of 10 μm on one side was cut by FIB and 0.8 μm thickness at the groove lines. The plastic deformation could be uses for the bending process of the cubic structure because the thickness of the groove line was higher than 0.5 μm. The fabricated thin-film graphite cubic net is shown in Figure 17a. One of the surfaces of the cubic net was bent by the end effector of a nanomanipulator (Figure 17(b)). The second, third, and fourth surfaces of the cubic net were bent in the same way (Figure 17c,17d and 17e). Fabrication of a thin-film graphite cubic structure using nanomanipulation was successful (Figure 17f). In this manner, a 3D structure of thin-film graphite was fabricated by bending using a nanomanipulator without breaking thin-film graphite.

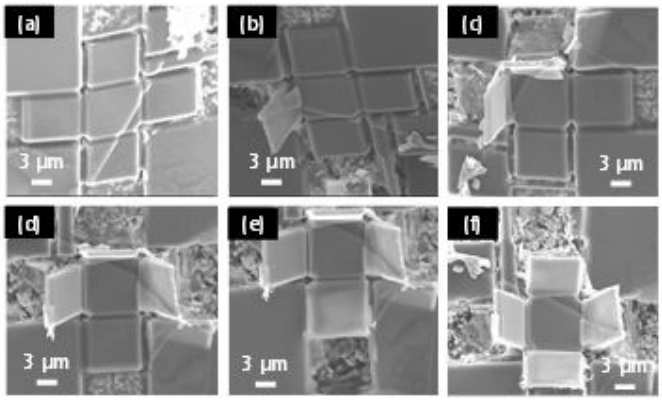

Figures 17(a-f): SEM images of fabrication 3D cubic structure. **(a)** Cutting as a cubic net design by FIB. **(b)** Bending of the one surface of cubic net. **(c)** Bending of the second surface of cubic net. **(d)** Bending of the third surface of cubic net. **(e)** Bending of the fourth surface of cubic net. **(f)** Fabricated 3D cubic structure.

Conclusion

A strategy to fabricate thin-film graphite with a cubic structure using nanomanipulation was presented. A nanomanipulator with three degrees of freedom was used to handle an end effector in a coordinated fashion. The mechanical properties of the bending process were evaluated using nanorobotic manipulation. In this study, the bending stress of thin-film graphite was also measured using a silicon cantilever to reveal the elastic and plastic deformation regions by bending manipulation. In this study, the spring constant is supposed by Hooke's law as the equation (1), and bending stress is supposed as the equation (2). For this experiment, a tungsten probe was used with FIB etching to adjust the size of the cubic net design for the bending process. From the experimental results, the

yield points changed depending on the thickness of the groove line. In this experiment, elastic deformation occurred in the thin-film graphite with a thickness of 0.4 μm or less, but plastic deformation occurred at a thickness of 0.5 μm. To fabricate the 3D structure, it is necessary to bring a plastic deformation for maintaining a deformation as a designed 3D structure, not an elastic deformation back to its original. From our experimental results, we conclude that it is required to conduct the bending nanomanipulation of thin-film graphite sheet with the thickness of 0.5 μm or more for obtaining around 90 degrees bending angle.

Finally, a cubic net was designed and fabricated using thin-film graphite by FIB etching, and each surface of the cubic net was bent to form a 3D cubic structure. In this paper, the width and length of one cubic net surface were designed to be 10 μm. The bending stress was also measured by bending manipulation of one surface of the cubic design using a silicon cantilever. By bending at an angle of more than 90°, the bending stress decreased slightly and then increased. From this bending point, the thin-film graphite was considered to undergo plastic deformation.

In future work, various 3D thin-film graphite structures will be fabricated using nanomanipulation based on the proposed method. It needs to reveal maximum bending angle by a bending test, since the graphite or graphene is considered to be brittle material basically. Additionally, a cycle test is required to obtain a fatigue strength. In another aspect, some additional supporting technique might be available to build certain shape micro-nano structures at the fabricated 3D structure. For example, EBID (Electron Beam Induced Deposition) can be considered as a proposal to improve durability [24,25]. It is considered that the durability can be improved by reinforcing the groove line and bent faces with the additional 3D structures. By applying the technique of this research, it is expected that thin-film graphite is applied into various 3D structures or 3D devices, such as four-sided pyramid and cylindrical column etc. various 3D structures [12], 3D devices such as nanosplit rings [13] and nanogripper opening and closing by electric [26].

References

1. Novoselov KS, Geim AK, Morozov SV, Jiang D, Zhang Y, et al. (2004) Electric Field Effect in Atomically Thin Carbon Film. Science 306: 666-669.
2. Daşdelen Z, Yıldız Y, Eriş S, Şen F (2017) Enhanced electrocatalytic activity and durability of Pt nanoparticles decorated on GO-PVP hybride material for methanol oxidation reaction. Applied Catalysis B: Environmental 219: 511-516.
3. Şen B, Lolak N, Paralı O, Koca M, Şen F (2017) Bimetallic PdRu/graphene oxide based Catalysts for one-pot three-component synthesis of 2-amino-4H-chromene derivatives. Nano-Structures & Nano-Objects 12: 33-40.
4. Demir E, Savk A, Sen B, Sen F, (2017) A novel monodisperse metal nanoparticles anchored graphene oxide as Counter Electrode for Dye-Sensitized Solar Cells. Nano-Structures & Nano-Objects 12: 41-45.
5. Bozkurt S, Tosun B, Sen B, Akocak S, Sen F (2017) A hydrogen peroxide sensor based on TNM functionalized reduced graphene oxide grafted with highly monodisperse Pd nanoparticles. Analytica chimica acta 989: 88-94.
6. Lee C, Wei X, Kysar JW, Hone J (2008) Measurement of the Elastic Properties and Intrinsic Strength of Monolayer Graphene. Science 321: 385-388.
7. Lee KJ, Chandrakasan AP, Kong J (2011) Breakdown Current Density of CVD-Grown Multilayer Graphene Interconnects. IEEE Electron Device Letters 32: 557-559.
8. Chen S, Wu Q, Mishra C, Kang J, Zhang H, et al. (2012) Thermal conductivity of isotopically modified graphene. Nature Materials 11: 203-207.
9. Scott Bunch J, van der Zande AM, Verbridge SS, Frank IW, Tanenbaum DM (2007) Electromechanical Resonators from Graphene Sheets. Science 305: 490-493.
10. Bernardi M, Palummo M, Grossman JC (2013) Extraordinary Sunlight Absorption and One Nanometer Thick Photovoltaics Using Two- Dimensional Monolayer Materials. Nano Lett 13: 3664-3670.
11. Song X, Oksanen M, Sillanpaa MA, Craighead HG, Parpia JM, et al. (2012) Stamp Transferred Suspended Graphene Mechanical Resonators for Radio Frequency Electrical Readout. Nano Lett 12: 198-202.
12. Yan Z, Zhang F, Wang J, Liu F, Guo X, et al. (2016) Controlled Mechanical Buckling for Origami-Inspired Construction of 3D Microstructures in Advanced Materials. Adv Funct Mater 26: 2629-2639.
13. Mao Y, Zhang W, Zhu R, Xu J, Wu W (2016) Multi-Direction-Tunable Three-Dimensional Meta-Atoms for Reversible Switching between Midwave and Long-Wave Infrared Regimes. Nano Lett 16: 7025-7029.
14. Fukuda T, Arai F, Dong LX (2003) Assembly of Nanodevices with Carbon Nanotubes through Nanorobotic Manipulations. In Proc of the IEEE 91: 1803-1818.
15. Nakajima M, Arai F, Fukuda T (2006) In situ Measurement of Young's Modulus of Carbon Nanotube inside TEM through Hybrid Nanorobotic Manipulation System. IEEE Transactions on Nanotechnology 5: 243-248.
16. Zimmermann S, Eichhorn V, Fatikow S (2012) Nanorobotic transfer and characterization of graphene flakes. In Proc. of 2012 IEEE/RSJ International Conference on Intelligent Robots and Systems (IROS 2012): 640 - 645.
17. Mashiyama D, Tobe T, Ogino T (2015) Nanopatterning of Suspended Graphene Films by Local Catalytic Etching Using Atomic Force Microscopy Equipped with an Ag-Coated Probe. J Phys Chem C 119: 11914-11921.
18. Liu L, Tan C, Chai J, Wu S, Radko A, et al. (2014) Electrochemically Writing Graphene from Graphene Oxide. Small 10: 3555-3559.
19. Dayen JF, Mahmood A, Golubev DS, Roch-Jeune I, Salles P, et al. (2008) Side-gated transport in FIB-fabricated multilayered graphene nanoribbons. Small 4: 716-720.
20. Lee C, Wei X, Kysar JW, Hone J (2008) Measurement of the Elastic Properties and Intrinsic Strength of Monolayer Graphene. Science 321: 385-388.

21. Rasool HI, Ophus C, Klug WS, Zettl A, Gimzewsk JK (2013) Measurement of the intrinsic strength of crystalline and polycrystalline graphene. Nature Communication 4: 2811.

22. Vasu KS, Rema K, Sampathc S, Sood AK (2013) Yield stress, thixotropy and shear banding in a dilute aqueous suspension of few layer graphene oxide platelets. Soft Matter 9: 5874-5882.

23. Scharfenberg S, Rocklin DZ, Chialvo C, Weaver RL, Goldbart PM, et al. (2011) Probing the mechanical properties of graphene using a corrugated elastic substrate. Applied Physics Letters 98: 091908.

24. Koops HWP, Kretz J, Rudolph M, Lee KL (1994) Characterization and Application of Materials Grown by Electron-Beam-Induced Deposition. Jpn J Applied Physics 33: 7099-7107.

25. Liu P, Arai F, Fukuda T (2006) Controlled nanowire growth with a nanorobotic manipulator Nanotechnology. Nanotechnology 17: 3023-3027.

26. Fujiwara T, Nakajima M, Ichikawa A, Hasegawa Y, Fukuda T (2017) Reversible Actuation of Folded Multilayered Graphene by Electrostatic Forces for Nano-gripper Application. Proc. of IEEENANO2017.